Multiple-wavelength conversion based on the anomalous Doppler effect induced by dynamic tuning in a self-collimation photonic crystal

Xingping Zhou,[1,2] Samit Kumar Gupta,[1,3] Guangxu Su,[1,2] Peng Zhan,[1,2,*] Minghui Lu,[1,3] and Zhenlin Wang[1,2,†]

[1]*National Laboratory of Solid State Microstructures and Collaborative Innovation Center of Advanced Microstructures, Nanjing University, Nanjing 210093, China*

[2]*School of Physics, Nanjing University, Nanjing 210093, China*

[3]*College of Engineering and Applied Sciences, Nanjing University, Nanjing 210093, China*

(Received 13 February 2019; published 16 July 2019)

The Doppler effect of relative motion-induced frequency shift as an interesting fundamental wave phenomenon draws significant research interest in many applied aspects of physics and engineering. Photonic settings represent an important class of platforms to observe and manipulate this effect. Here, an anomalous Doppler effect via dynamic index tuning in a photonic crystal (PhC) is proposed and investigated theoretically by considering the guided reflection of light from a moving front at near the speed of light. A virtual waveguide constructed in a square lattice PhC slab utilizing the self-collimation effect is proposed, and the moving equivalent reflector is realized by photonic band shift induced by a pump light for changing the refractive index dynamically. The anomalous Doppler shift occurs at multiple wavelengths, which depends on the Bloch nature of this photonic crystal and its band structure. Moreover, another kind of small spectral shift caused by adiabatic wavelength conversion is also observed. This nonstationary procedure is studied combining the full-wave numerical simulation and wavelet transform analysis. This work sheds light on the emergence of anomalous Doppler effect and wavelength conversion via dynamic index tuning in photonic crystals and can be important for manipulating such effects in practical photonic devices.

DOI: 10.1103/PhysRevA.100.013830

I. INTRODUCTION

The Doppler effect is a fundamental frequency shift phenomenon caused by relative motion between wave source and observer, which has well-established applications in satellite global positioning systems, weather and aircraft radar systems, biological diagnostics, and astrophotonics [1]. Doppler effects which occur in the cases of moving mirrors [2], propagating dielectric interfaces [3], and ionization fronts [4] have been widely investigated theoretically and experimentally. Photonic crystal (PhC) provides an important research platform for the Doppler effect, and later, anomalous Doppler shifts have also been found to occur when an oscillating dipole moves in photonic crystals and other periodic media [5–10]. Very recently, the anomalous Doppler effect induced by dynamic tuning on a PhC waveguide was reported by Kondo and Baba [10]. While the anomalous Doppler effects can be predicted by the phase continuity and the photonic band theory, in the case of conventional Doppler frequency shift, the observed frequency is higher (lower) compared to the emitted frequency during moving toward (away from) the observation point. Since the Bloch waves in a periodic structure can be represented as a sum of discrete plane waves, multiple wavelengths will be generated in the frame moving with the front [7]. Most of the photonic transition and its corresponding applications are achieved by a photonic crystal waveguide platform utilizing the waveguide mode (the defect mode) which is the photonic band of a superlattice with a line defect [10–13]. In fact, this process can occur in any photonic band. In this article, we demonstrate the photonic transition in the bulk photonic band and the associated anomalous Doppler effect that results from it.

PhCs have complex spatial dispersion properties which can provide mechanisms to control the flow of light at subwavelength scale. One of the most intriguing effects is the self-collimation by which a beam of an electromagnetic wave can propagate with almost no diffraction in a perfectly periodic PhC instead of introducing a line defect. It was first found by Kosaka *et al.* [14], and has been used to construct virtual waveguides or beam splitters by several other groups [15–18]. Here, we theoretically study the Doppler effect of a propagating light along the virtual waveguide based on the self-collimation effect in planar square PhC lattices. In this proposed system, the moving "mirror" is defined by the photonic band shift through a spatiotemporal modulation process. Spectral reflection dependent on different velocities (v_m) of a moving "mirror" illustrates the anomalous Doppler effect, which is induced by the Bloch nature of this photonic lattice crystal and could be predicted by the intersections of the phase continuity and the photonic band. In addition, another kind of small spectral shift also occurs due to the adiabatic wavelength conversion. As the anomalous Doppler effect is a nonstationary process that has a variable frequency over time, the Fourier transform cannot provide the information of time. In order to ameliorate this aspect, the wavelet transform has been utilized to analyze this

*zhanpeng@nju.edu.cn
†zlwang@nju.edu.cn

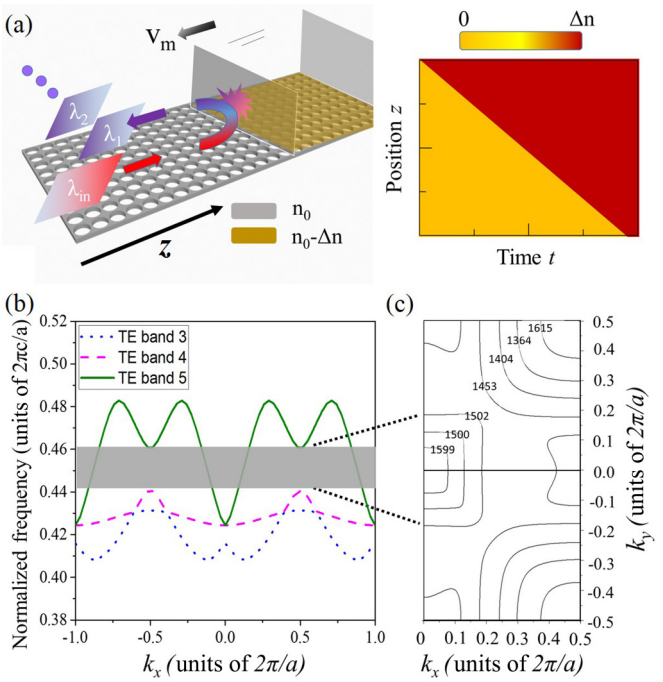

FIG. 1. (a) Schematic diagram of the theoretical setup. The right panel stands for the spatiotemporal change in $|\Delta n|$. It shows the process of the spatiotemporal dynamic tuning on PhC. $a = 702$ nm is the lattice constant. (b) Band diagram of the third, fourth, and fifth TE bands. The self-collimation effect can occur at the normalized frequencies in the gray-shaded area. (c) Equifrequency contour (EFC) for the PhC structures of the fifth TE band.

nonstationary optical process combining the full-wave numerical simulation.

II. RESULTS AND DISCUSSIONS

The structure of the PhC considered herein is shown in Fig. 1(a), which consists of a square lattice of air holes (141×23) introduced into a high-index material with a lattice constant of $a = 702$ nm. The normalized hole diameter is set as $2r/a = 0.59$. We assume that the effective refractive index of this slab is $n_0 = 2.963$ (modal equivalent index of a 260-nm-thick freestanding nanostructured Si slab with an index of 3.5 at $\lambda = 1550$ nm [10]). Because the propagation direction of light in PhCs is the direction of its group velocity, $v_g = \nabla_k \omega(k)$, the direction of the group velocity can be determined by the gradient direction of the corresponding Equifrequency contour (EFC) [14]. Therefore, the self-collimation effect can be achieved by having flat EFCs (we use a free and open-source software package MPB [19]) in the dispersion relation of the PhCs. Shown as the constant-wavelength contour representation of the fifth band for the TE modes in Fig. 1(c) (the TE modes have the electric fields perpendicular to the axis direction of the air holes), such a lattice structure provides wide-angle self-collimated propagation along the x direction for the wavelength in the vicinity of 1550 nm. We can set the signal pulse at wavelength $\lambda_{in} = 1550$ nm which propagates from left to right as shown schematically in Fig. 1(a). By launching an intense control pulse propagating along the Si

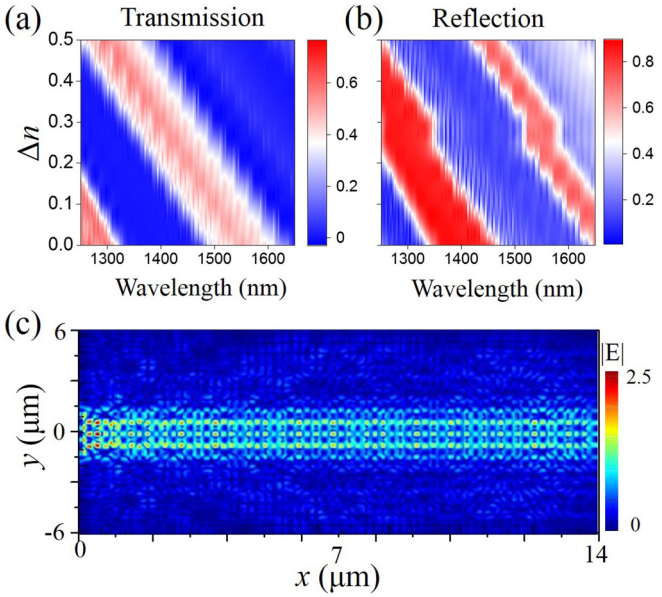

FIG. 2. (a,b) The transmission and reflection spectra of the setup shown in Fig. 1(a). (c) The electric field as a self-collimated beam propagating from left to right.

PhC from right to left, which produces spatiotemporal index dynamic tuning [20], we can construct a moving mirror as shown in Fig. 1(a) as the refractive index of Si changes. The mirror can also be considered essentially as a moving source of light, which emits light at a particular frequency. Due to different group velocities in the EFC, we can change the speed of the moving mirror by adjusting the wavelength. It can also be realized by electro-optical effect [13] to a growing periodic structure with velocities close to the speed of light in a medium. Here, the moving front is described by the time-varying material. However, it necessitates a large index change during this process. In this case, InP, a semiconductor material [21], or chalcogenide glass [22], which can offer a larger index change of 0.01, may be useful.

To quantify the diffraction behaviors of the self-collimated beams, we truncate the crystal at a (10) surface, and place a line monitor behind a source with a width of $5a$ to obtain the reflection spectrum. Another line monitor is placed on the other side of the crystal to obtain the transmission spectrum. A pulse consisting of the fundamental mode of the virtual waveguide is then excited and incident upon the crystal. We monitor the propagation properties of the beam thus generated inside the crystal to get the transmission and reflection spectra [plotted in Figs. 2(a) and 2(b)] through the Finite-Difference Time-Domain (FDTD) method. It is obvious that the wavelength region of wide-angle self-collimated propagation is apparently dependent on Δn, which is defined as the value of the reduced index after dynamic tuing. As Δn increases, the high transmission band shows a blueshift, and thus the signal pulse with $\lambda_{in} = 1550$ nm enters the non-self-collimation region. Figure 2(c) shows the typical electric field distribution of the guiding wave for specific wavelength at $\lambda_{in} = 1550$ nm when $\Delta n = 0$. It is evident that self-collimation occurs due to which it forms a virtual waveguide similar to the waveguide formed by a line defect.

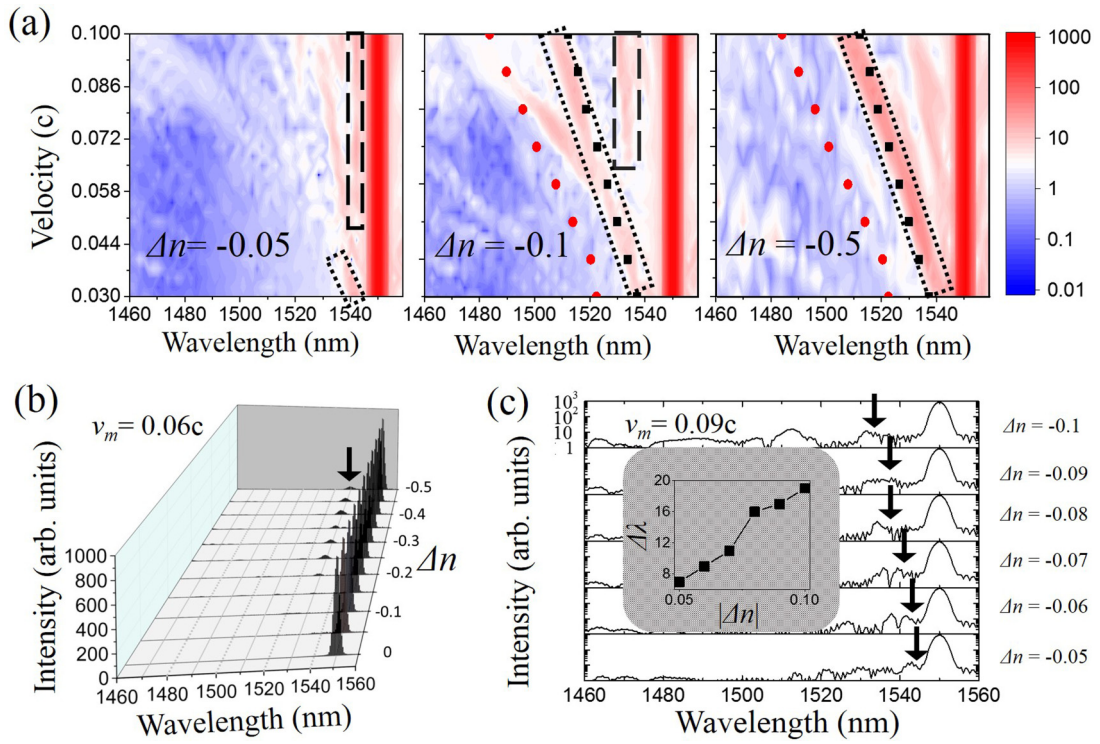

FIG. 3. (a) Calculated signal spectra. Excitation is given around the wavelength centered at $\lambda_{in} = 1550$ nm, which corresponds to $k_x = 0.87$ shown in Fig. 1(b). Here, c is the velocity of light in vacuum and for simplicity we set $c = 3 \times 10^8$ m/s. The temporal full width at half maximum of the initial pulse is 1.6 ps. (b) The signal spectra of different Δn but the same velocity $v_m = 0.06c$. (c) The signal spectra corresponding to different Δn but at the same velocity $v_m = 0.09c$.

Mathematically, the spatiotemporal refractive index distribution in Fig. 1(a) can be described by

$$n(z,t) = n_0 + \Delta n[u(z - z_0 + v_m t)]. \quad (1)$$

Here, $u(x)$ stands for the step function and z_0 is the position of the right edge of the sample shown in Fig. 1(a). Figure 3(a) shows the spectral reflection of the signal pulse calculated by Fourier transform in the frequency domain for different values of Δn and v_m. We put the monitor near the place of excitation along the direction of light propagation, so that the spectral peaks from the excitation source and reflected pulse both can be observed. The spectra indicated by the rectangular dotted frame show that the blueshift increases with $|v_m|$. This Doppler phenomenon arises due to the effects produced by the moving periodic structure and can be predicted by [9,10]

$$\omega' = \omega_{in} + v_m(k - k_{in} - G_r). \quad (2)$$

ω_{in} and k_{in} represent the frequency and wave vector of the input source, respectively. G_r is an integer number which stands for the reciprocal lattice vector; hence different G_r can induce multiple ω'. After interacting with the front, only the modes exist that fulfill Eq. (2) which means that only frequencies can be observed for which the mode dispersion function intersects with the lines. The black and red dots in Fig. 3(a) represent wavelength shifts obtained from Eq. (2) (intersections of the lines and the bands of the PhC) with $k_{in} = 0.87$, while the black and red dots are for $G_r = 0$ and -1, respectively. It can be seen from Fig. 3(a) that the peaks for $G_r = 0$ are larger in intensity but have less wavelength shift which is called the nonadiabatic Doppler shift [6]. We can see that the peaks for $G_r = -1$ (indicated by red dots) are much smaller in intensity but have more wavelength shift which occurs through the continuous intraband transition [10]. It can be seen from Fig. 3(a) that the Doppler shift occurs more easily when $|\Delta n|$ is large (shown in the dotted line boxes). As shown in Fig. 3(a), the wavelength shifts obtained from FDTD simulation and Eq. (2) are in good agreement, especially those corresponding to $G_r = 0$. According to Eq. (1), the wavelength shift depends on the v_m instead of the Δn. To see this point, we give the spectra of different Δn ranging from 0 to -0.5 but the same velocity $v_m = 0.06c$ in Fig. 3(b) in which as the $|\Delta n|$ increases, the Doppler peak around 1529 nm emerges and remains unchanged (indicated by the black arrow).

Except for those peaks which can be expected by Eq. (2), there are peaks (indicated by the rectangular wire frames) that do not conform to this. We can call those as extended Doppler shifts induced by a moving dielectric boundary [10].The signal pulse backpropagates but cannot go ahead of the mirror (the moving wall), so those peaks depend more on the Δn instead of the v_m. We can see from Fig. 3(a) that those peaks remain unchanged as the v_m increases. While we keep the v_m unchanged ($v_m = 0.09c$) and let the $|\Delta n|$ increase from 0.05 to 0.1 [shown in Fig. 3(c)], blueshifts are found for those peaks which can be seen more clearly from the inset. Actually, they can be better understood by adiabatic wavelength conversion induced by dynamic tuning [9,10,20] because of the continuing interaction between the signal pulse and index change.

III. WAVELET TRANSFORM

Since dynamic tuning is performed in the time domain, and the frequency of light waves changes over time, the Fourier transform–based mathematical formulation loses time-domain information while performing frequency- to time-domain conversion. In effect, Fourier transform can only provide frequency-domain information and not the time-domain information of these frequencies. In other words, there are limitations to the nonstationary process by Fourier transform. To overcome this particular issue, the short-time Fourier transform (STFT) is proposed [23]. It is worth noting that while the STFT can be used to analyze the piecewise stationary signal or the approximate stationary signal, for the nonstationary signal, especially when the signal changes rapidly, the window function is required to have a higher temporal resolution. On the other hand, when the waveform changes slightly, for example, the low-frequency signal, the window function is required to have a higher-frequency resolution. But in such cases, STFT cannot meet the requirement of simultaneous frequency- and time-domain resolution. Under the situation, it is found that the wavelet analysis can be a useful tool that can effectively address this issue [24,25]. Compared with Fourier transform, the wavelet transform is a local transform in time and frequency domain, so that it can extract information from signals effectively. Multiscale analysis is carried out on functions or signals through scaling and shifting, which solves several limitations imposed by Fourier transform and STFT.

The wavelet transform formula is

$$WT(a,\tau) = \frac{1}{\sqrt{a}} \int_{-\infty}^{\infty} f(t)\psi\left(\frac{t-\tau}{a}\right)dt. \tag{3}$$

We note that unlike Fourier transform, wavelet transform has two variables: scale and translation. While the scale a controls the scaling of the wavelet function, the translation τ is related to the frequency domain of the wavelet function. The scale corresponds to the frequency (inverse ratio), and the translation corresponds to time. In this way, the wavelet transform can obtain a time-frequency spectrum, in contrast to the Fourier transform where only the frequency spectrum can be obtained. We note that for smooth continuous wavelet amplitude, the nonorthogonal wavelet function is more suitable. In our work, the Morlet wavelet transform is employed, which can be given by

$$\psi_0(t) = \pi^{-1/4} e^{i\omega_0 t} e^{-t^2/2}, \tag{4}$$

where t is time and ω_0 is dimensionless frequency. We apply the Morlet wavelet Eq. (4) to Eq. (3) to obtain

$$WT(a,\tau) = \pi^{-1/4} a^{-1/2} \int_{-\infty}^{\infty} f(t) e^{i\omega_0\left(\frac{t-\tau}{a}\right) - \left(\frac{t-\tau}{a}\right)^2/2} dt. \tag{5}$$

For brevity, we only perform the wavelet transform on the signal of $\Delta n = -0.5$ and $v_m = 0.1c$. We set a line monitor alone the direction of the light to record the intesity with the time. The result has been depicted in Fig. 4(a). The horizontal axis is the geometrical coordinates in the x direction and the longitudinal axis represents the time axis. As the temporal full width at half maximum (FWHM) of the initial pulse is 1.6 ps, the light beam has a bandwidth around 3.5 ps. We can see

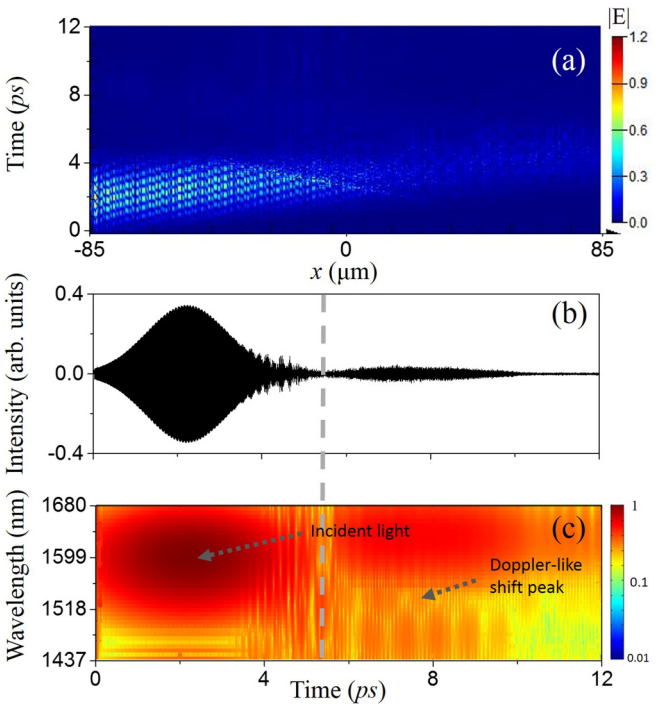

FIG. 4. (a) The field intensity of the line alone the direction of the light. (b) Amplitude observed near the excitation source. (c) Wavelet transform of the signal in (b).

an oblique line at about 4 ps, where the Doppler effect and wavelength conversion occurs. After the moment, the input light is reflected. The signal of the point monitor near the input source is shown in Fig. 4(b), while the first peak refers to the input source and the second one corresponds to the reflected signal. Obviously, the frequency or wavelength of these two peaks is different as shown in Fig. 3, which is performed by Fourier transform. Then we use the complex Morlet function as the wavelet function to perform the wavelet transform on the signal of time domain [plotted in Fig. 4(b)]. The result is shown in Fig. 4(c) in which the horizontal axis is the time axis and the longitudinal axis represents the wavelength range. It can be seen that before 4.3 ps, there is only the 1550-nm component of incident light. After 4.3 ps, the Doppler peak appears (indicated by the gray arrow).

IV. SUMMARY

In conclusion, we have discussed the Doppler effect in a perfectly periodic PhC in which the moving mirror is generated by the photonic band shift induced by dynamic tuning and light travels along a virtual waveguide formed by self-collimation. We show that the bulk photonic band can also be employed to realize the transition of the operating point. Signal spectra with different values of Δn and v_m are demonstrated to illustrate the effects of the index tuning and the relative motion of the moving source of light on the Doppler effect. We show two different kinds of shifts in our photonic lattice. While the anomalous Doppler shift is induced by the Bloch nature of the photonic crystal, an additional small shift arises due to the adiabatic wavelength conversion. We show that the bulk state in the photonic bands can also lead to the anomalous Doppler effect the same as

the waveguide mode (the defect state). We also demonstrate how the wavelet transform can be used to analyze the signal reflected by the moving mirror. The wavelet transform used in our work further describes the changes in the Doppler effect for our nonstationary signal. Our work may be useful in studies pertaining to wavelength conversion of light for applications in optical information processing [26–28].

ACKNOWLEDGMENTS

The authors express thanks for the support by the National Key R&D Program of China (2017YFA0303702, 2018YFA0306202) and the National Science Foundation of China under Grants No. 11834007, No. 11674166, No. 11674168, No. 11774162, and No. 11621091.

[1] T. P. Gill, *The Doppler Effect: An Introduction to the Theory of the Effect* (Academic Press, New York, 1965).
[2] H. E. Ives, The Doppler effect from moving mirrors, J. Opt. Soc. Am. **30**, 255 (1940).
[3] C. Tsai and B. Auld, Wave interactions with moving boundaries, J. Appl. Phys. **38**, 2106 (1967).
[4] M. Lampe, E. Ott, and J. H. Walker, Interaction of electromagnetic waves with a moving ionization front, Phys. Fluids **21**, 42 (1978).
[5] E. J. Reed, M. Soljačić, and J. D. Joannopoulos, Color of Shock Waves in Photonic Crystals, Phys. Rev. Lett. **90**, 203904 (2003).
[6] E. J. Reed, M. Soljačić, and J. D. Joannopoulos, Reversed Doppler Effect in Photonic Crystals, Phys. Rev. Lett. **91**, 133901 (2003).
[7] E. J. Reed, M. Soljačić, M. Ibanescu, and J. Joannopoulos, Reversed and anomalous Doppler effects in photonic crystals and other time-dependent periodic media, J. Comput.-Aided Mater. Des. **12**, 1 (2005).
[8] C. Luo, M. Ibanescu, E. J. Reed, S. G. Johnson, and J. D. Joannopoulos, Doppler Radiation Emitted by an Oscillating Dipole Moving inside a Photonic Band-Gap Crystal, Phys. Rev. Lett. **96**, 043903 (2006).
[9] E. A. Ulchenko, D. Jalas, A. Y. Petrov, M. C. Muñoz, S. Lang, and M. Eich, Pulse compression and broadening by reflection from a moving front of a photonic crystal, Opt. Express **22**, 13280 (2014).
[10] K. Kondo and T. Baba, Slow-light-induced Doppler shift in photonic-crystal waveguides, Phys. Rev. A **93**, 011802(R) (2016).
[11] M. Castellanos Muñoz, A. Y. Petrov, L. O'Faolain, J. Li, T. F. Krauss, and M. Eich, Optically Induced Indirect Photonic Transitions in a Slow Light Photonic Crystal Waveguide, Phys. Rev. Lett. **112**, 053904 (2014).
[12] D. M. Beggs, I. H. Rey, T. Kampfrath, N. Rotenberg, L. Kuipers, and T. F. Krauss, Ultrafast Tunable Optical Delay Line Based on Indirect Photonic Transitions, Phys. Rev. Lett. **108**, 213901 (2012).
[13] H. Lira, Z. Yu, S. Fan, and M. Lipson, Electrically Driven Nonreciprocity Induced by Interband Photonic Transition on a Silicon Chip, Phys. Rev. Lett. **109**, 033901 (2012).
[14] H. Kosaka, T. Kawashima, A. Tomita, M. Notomi, T. Tamamura, T. Sato, and S. Kawakami, Self-collimating phenomena in photonic crystals, Appl. Phys. Lett. **74**, 1212 (1999).
[15] X. Yu and S. Fan, Bends and splitters for self-collimated beams in photonic crystals, Appl. Phys. Lett. **83**, 3251 (2003).
[16] Y. Zhang, Y. Zhang, and B. Li, Optical switches and logic gates based on self-collimated beams in two-dimensional photonic crystals, Opt. Express **15**, 9287 (2007).
[17] S.-G. Lee, S. S. Oh, J.-E. Kim, H. Y. Park, and C.-S. Kee, Line-defect-induced bending and splitting of self-collimated beams in two-dimensional photonic crystals, Appl. Phys. Lett. **87**, 181106 (2005).
[18] L. Gan, F. Qin, and Z.-Y. Li, Broadband large-angle self-collimation in two-dimensional silicon photonic crystal, Opt. Lett. **37**, 2412 (2012).
[19] S. G. Johnson and J. D. Joannopoulos, Block-iterative frequency-domain methods for Maxwell's equations in a planewave basis, Opt. Express **8**, 173 (2001).
[20] M. Notomi and S. Mitsugi, Wavelength conversion via dynamic refractive index tuning of a cavity, Phys. Rev. A **73**, 051803(R) (2006).
[21] B. R. Bennett, R. A. Soref, and J. A. Del Alamo, Carrier-induced change in refractive index of InP, GaAs and InGaAsP, IEEE J. Quantum Electron. **26**, 113 (1990).
[22] K. Suzuki and T. Baba, Nonlinear light propagation in chalcogenide photonic crystal slow light waveguides, Opt. Express **18**, 26675 (2010).
[23] J. Allen, Short term spectral analysis, synthesis, and modification by discrete Fourier transform, IEEE Trans. Acoust., Speech, Signal Process. **25**, 235 (1977).
[24] Y. Meyer and R. Coifman, *Wavelets: Calderón-Zygmund and Multilinear Operators*, Cambridge Studies in Advanced Mathematics Vol. 48 (Cambridge University Press, Cambridge, 1997).
[25] I. Daubechies, *Ten Lectures on Wavelets* (Society For Industrial and Applied Mathematics, Philadelphia, 1992).
[26] J. M. Elmirghani and H. T. Mouftah, All-optical wavelength conversion: technologies and applications in DWDM networks, IEEE Commun. Mag. **38**, 86 (2000).
[27] B. Ramamurthy and B. Mukherjee, Wavelength conversion in WDM networking, IEEE J. Sel. Areas Commun. **16**, 1061 (1998).
[28] S. B. Yoo, Wavelength conversion technologies for WDM network applications, J. Lightwave Technol. **14**, 955 (1996).